Biomedical Physics & Engineering Express

ENDORSED BY IPEM Institute of Physics and Engineering in Medicine

PAPER • OPEN ACCESS

SAXS-CT: a nanostructure resolving microscopy for macroscopic biologic specimens

To cite this article: A L C Conceição *et al* 2020 *Biomed. Phys. Eng. Express* **6** 035012

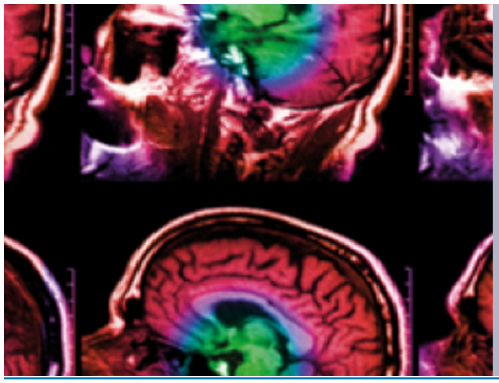

Biomedical Physics & Engineering Express

OPEN ACCESS

RECEIVED
11 December 2019

REVISED
20 February 2020

ACCEPTED FOR PUBLICATION
4 March 2020

PUBLISHED
26 March 2020

PAPER

SAXS-CT: a nanostructure resolving microscopy for macroscopic biologic specimens

A L C Conceição[1,2], **J Perlich**[1,3], **S Haas**[1] and **S S Funari**[1]

[1] Deutsches Elektronen-Synchrotron DESY, Notkestraße 85, D-22607 Hamburg, Germany
[2] Federal University of Technology - Paraná, Av. Sete de Setembro 3165, 80230-901 Curitiba, Brazil
[3] Present address: Continental Reifen Deutschland GmbH, Jädekamp 30, D-30419 Hanover, Germany.

E-mail: andre.conceicao@desy.de

Keywords: SAXS, computed tomography, nanostructural mapping, breast cancer

Abstract

SAXS-CT is an emerging powerful imaging technique which bridges the gap between information retrieved from high-resolution local techniques and information from low-resolution, large field-of-view imaging, to determine the nanostructure characteristics of well-ordered tissues, *e.g.*, mineralized collagen in bone. However, in the case of soft tissues, features such as poor nanostructural organization and high susceptibility to radiation-induced damage limit the use of SAXS-CT. Here, by combining the freeze-drying the specimen, preceded by formalin fixation, with the nanostructure survey we identified and monitored alterations on the hierarchical arrangement of triglycerides and collagen fibrils three-dimensionally in breast tumor specimens without requiring sample staining. A high density of aligned collagen was observed precisely on the invasion front of the breast carcinoma, showing the direction of cancer spread, whereas substantial content of triglycerides was identified, where the healthy tissue was located. Finally, the approach developed here provides a path to high-resolution nanostructural probing with a large field-of-view, which was demonstrated through the visualization of characteristic nanostructural arrangement and quantification of content and degree of organization of collagen fibrils in normal, benign and malignant human breast tissue.

Introduction

The development of new technologies reaching nano dimensions promises a significant impact on human health issues. In nanomedicine, the expected breakthroughs are human organ restoration using engineered tissue (Isenberg and Wong 2006), 'designer' drugs created from directed assembly of atoms and molecules (Huang *et al* 2014) as well as an urgent need for personalized targeted treatments for diseases like cancer (Jackson and Chester 2015, National Research Council US Committee on a Framework for Developing a New Taxonomy of Disease 2011, since personalized treatment directed to molecular targets should improve outcome for patients with poor prognosis (Chantrill *et al* 2015). However, these goals are strongly dependent on extensive knowledge of the molecular and supramolecular structural profiling of soft tissues.

Currently, researchers use techniques such as atomic force microscopy (AFM) (Jorba *et al* 2017), transmission electron microscopy (TEM) (Peddie and Collinson 2014) and second-harmonic generation (SHG) (Brown *et al* 2003) for that purpose. These techniques require complex sample preparation and/or analyze a very small field-of-view. Alternatively, the availability of brighter x-ray sources, fast and essentially noise-free detectors and automated analysis schemes, enable a new favorable context for the development of high-resolution tomography-based techniques (Bleuet *et al* 2008, Antoniassi *et al* 2014, Manohar *et al* 2016, Romanov *et al* 2017).

Combining small-angle x-ray scattering (SAXS), a powerful analytical tool, with computed tomography (CT) a well-established imaging technique that provides access to volume-resolved information, the spatially resolved content and structural organization of embedded structures at the nanoscale can be retrieved three-dimensionally. SAXS-CT bridges the gap between information retrieved from high-resolution local techniques and information from low-resolution, large field-of-view imaging techniques (Schroer *et al* 2006, Stribeck *et al* 2006, 2008, Fratzl 2015). In

addition, SAXS-CT has the advantage of *ex vivo* tissue specimen experiments without the requirement for staining samples with specific dyes.

Although SAXS-CT has been used to improve the contrast of brain tumor in rats by using the slope of the scattering curves (Jensen *et al* 2011) as well as to investigate mineralized collagen in rigid samples like bone (Georgiadis *et al* 2015, Liebi *et al* 2015, 2018) and tooth (Schaff *et al* 2015, Sharma *et al* 2016), to the best of the authors' knowledge, this approach for spatially resolved identification and mapping of nanostructure changes in soft tissue has not been undertaken before. Among the challenges to applying SAXS-CT on soft matter, undoubtedly, the poor nanostructure organization comparative to bone specimens and the avoidance of radiation-induced damage are the major challenges. In general, soft tissues are poorly organized and inhomogeneous which might imply amorphous phases and thus complicates the selection of single Bragg diffraction peaks necessary for image reconstruction.

To overcome the limitations of using SAXS-CT to investigate soft tissue, freeze-dried normal and pathological human breast specimens, preceded by formalin fixation were prepared for this study. Freeze-drying, also called lyophilization, involves snap freezing a sample, lowering the pressure, and then removing ice by sublimation. This process removes a high percentage of water from the sample (more than 99% depending on the type of sample) while retaining its structural and molecular integrity (Jennings 1999) and has the advantage of being reproducible if tissue thickness and lyophilization time are kept constant (Png *et al* 2008). Consequently, the susceptibility to radiation damage is sharply reduced as well as the SAXS contrast is improved because water is absent and the spatial electron density is now related to the remaining dry mass only (Zierold 1988).

Therefore, this paper will present the potential of SAXS-CT as a nanostructural resolving microscopy on investigating human tissue specimens. We demonstrate the approach by focusing our experimental protocol on how to identify and monitor alterations on the hierarchical arrangement of nanostructures compliant to benign and malignant human breast disease progression through a macroscopic specimen without requiring any specific dye.

Methods

Sample collection and classification

Three human breast specimens classified as normal, benign and malignant lesions were investigated. Pathological tissues were taken from patients who had mammographically, ultrasonographically and biopsy confirmed lesions, while the normal specimen was obtained after reduction mammoplasty in the Clinics Hospital of the Ribeirão Preto Medical School, University of São Paulo, Ribeirão Preto, Brazil. The Ethics Review Board on Human Research at the Ribeirão Preto General Hospital and Ribeirão Preto Medical School following the guidelines of the Declaration of Helsinki and its revisions approved this study. Just after excision, each specimen was cut in a cylindrical shape with 0.8 mm in diameter and 5 mm in height. A thin disk was cut from the cylinder to obtain prior histopathology information about the samples. This disk was immediately processed and sliced for histological examination under the microscope. An experienced breast pathologist directed this examination. The information obtained was taken as a guideline for the SAXS-CT experiment, allowing to select the region-of-interest. The normal specimen was composed of approximately 90% of adipose tissue with the remaining of fibroglandular tissue. The benign lesion was classified as fibroadenoma, whereas the malignant sample as grade-III Invasive Ductal Carcinoma. Subsequently, the specimens were stored, at room temperature, into the suitable receptacles and fixed in neutral buffered formalin (NBF).

SAXS scanning

For breast tissues, the water content represents more than 60% in mass (Graham *et al* 1995). Water molecules are very susceptible to radiolysis, leading to radiation-induced damage to the tissue structure. SAXS scanning on normal and pathological human breast tissues was conducted on samples solely formalin-fixed as well as further freeze-drying to evaluate the impact on the hierarchical tissue arrangement while minimizing radiation damage. Each sample was inserted into a holder and positioned accurately to carry out the SAXS scanning. This experiment was performed at the D02A-SAXS2 beamline in the National Synchrotron Light Laboratory in Campinas, Brazil. Three SAXS images were recorded for each breast specimen at both states, native (formalin-fixed only) and lyophilized, on a MarCCD 165 detector with 2048 $\times$ 2048 pixels, pixel-size of 79 μm and protected by a 6 mm-diameter beam stop. The x-ray beam (0.5 $\times$ 0.2 mm^2 and wavelength of 1.608 Å) passing through the vertical axis of the cylinder and two others adjacent to this, separated by 0.2 mm. These recorded images were summed up to obtain an average scattering profile of the sample. A sample-to-detector distance of 1602 mm was used to register the momentum transfer range of $0.17\ \mathrm{nm}^{-1} < q\ (=4\pi\sin(\theta/2)/\lambda) < 1.76\ \mathrm{nm}^{-1}$, where θ is the scattering angle and λ the wavelength.

Sample freeze-drying

To minimize radiation damage as well as volume variation during the SAXS-CT experiment, the residual water content of the formalin-fixed samples was removed by freeze-drying (or lyophilization) using a lyophilizer Terroni® LS 3000. The following steps were taken: (1) freezing the sample at −50 °C for 8 h; (2) primary drying −50 °C for 48 h; and (3) secondary

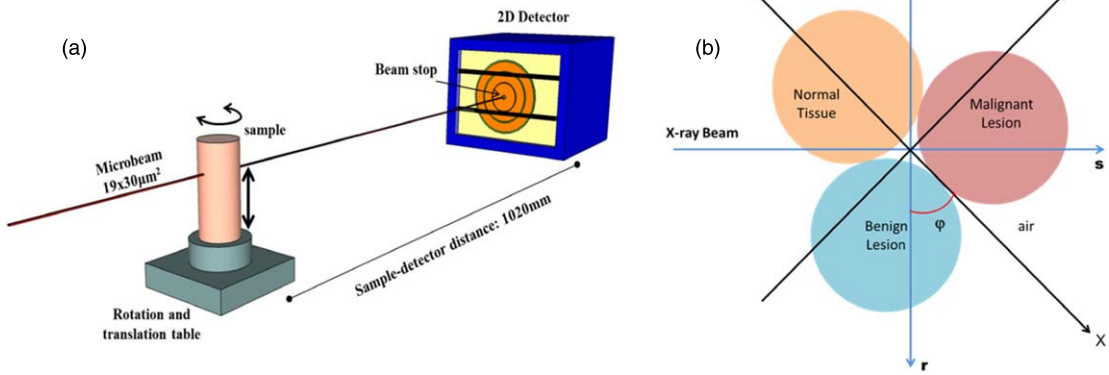

Figure 1. SAXS-CT experiment. (a) Schematic representation of the experimental setup for SAXS-CT; (b) top view of the sample assembly as the specimens were mounted and the coordinate system of the experiment. A detailed description of the instrument is presented by Roth and coworkers (Roth *et al* 2006).

drying at 25 °C for 24 h. The chamber pressure was maintained at 20 Pa during the drying process. When the lyophilization process was over, the vials were immediately filled with nitrogen gas, sealed with rubber caps, and stored at 4 °C. Just before a new SAXS scanning and SAXS-CT experiments, the dried specimens were brought to room temperature.

SAXS-CT approach

The three dried human breast specimens were put together to compose the investigated assemble. The experiments were carried out in the beamline BW4 at the synchrotron radiation facility DORIS III in Hamburg, Germany (Roth *et al* 2006). Figure 1(a) compiles the experimental setup. Monochromatic x-rays with a wavelength of 1.38 Å and a beam size of 19 × 30 μm^2 were focused on the sample mounted on a stage with the orthogonal translations s and r and the rotation φ around the vertical axis through the center of the assembly. The SAXS patterns were recorded with a Pilatus 300 k detector, using a sample-to-detector distance of 2320 mm corresponding to a q-range 0.08 nm^{-1} ⩽ q ⩽ 1.71 nm^{-1}. 5760 SAXS patterns were acquired for 16 steps equally spaced in 100 μm along the r axis in figure 1(b) and 360° with 1° step size, using a exposure time of 10 s for each pattern following the methodology previously reported (Schroer *et al* 2006, Stribeck *et al* 2008, Feldkamp *et al* 2009). A set of two pin-diodes, placed before the sample and adjacent to the beam stop, were used to monitor primary and transmitted beam intensities, respectively.

SAXS-CT requires long radiation exposure and visible changes in scattered intensity and collagen ordering for absorbed doses above 10^5 Gy has been reported (Fernández *et al* 2002). To control this issue, the radiation dose was kept below 800 Gy per SAXS pattern while ensuring statistically significant contrast and the irradiated specimen position was changed regularly to provide a longer time for biological repair.

Data treatment and image reconstruction

Assuming the sample scatters isotropically, as is expected for triglycerides and randomly oriented collagen fibrils in breast tissue and only the scattering in the q_z direction is reconstructed, the scattered intensity at a specific momentum transfer can be considered as scalar. This last assumption relies on the fact that in breast tumor the collagen fibrils are arranged either parallel or perpendicular to the tumor cell membrane (Provenzano *et al* 2006), so the tumor specimens were cut at the sagittal plane of the tumor preferential growth direction guided by the expert pathologist. Thereby, we assume that the scattering is along the z-axis. In addition. it is important to mention here that in case we were interested in determining the preferred orientation of such structures, another approach must be adopted (Skjønsfjell *et al* 2016, Liebi *et al* 2018). Then, the full scattering intensity from a sample $I(r, \varphi, q)$ at coordinate (r, φ) as function of $q = (q_r, q_z)$ can be described as following:

$$I(r, \varphi, q) = I_0 \int e^{-\int_{-\infty}^{s} \mu[x(s',r),y(s',r)]ds'} p_{q,\varphi}[x(s', r), y(s', r)] \times e^{-\int_{s}^{\infty} \mu[x(s',r),y(s',r)]ds'} \Delta\Omega \, ds \quad (1)$$

where I_0 is the incident intensity, $p_{q,\varphi}$ is the SAXS cross section at a certain location (x, y) with the sample rotated by the angle φ. The exponential functions before and after the SAXS cross section parameter describe the attenuation of the incident and forward scattered beams, respectively.

SAXS tomograms are reconstructed from the recorded SAXS patterns as shown on the workflow in figure 2. The recorded SAXS patterns were corrected by self-attenuation, scattering background,

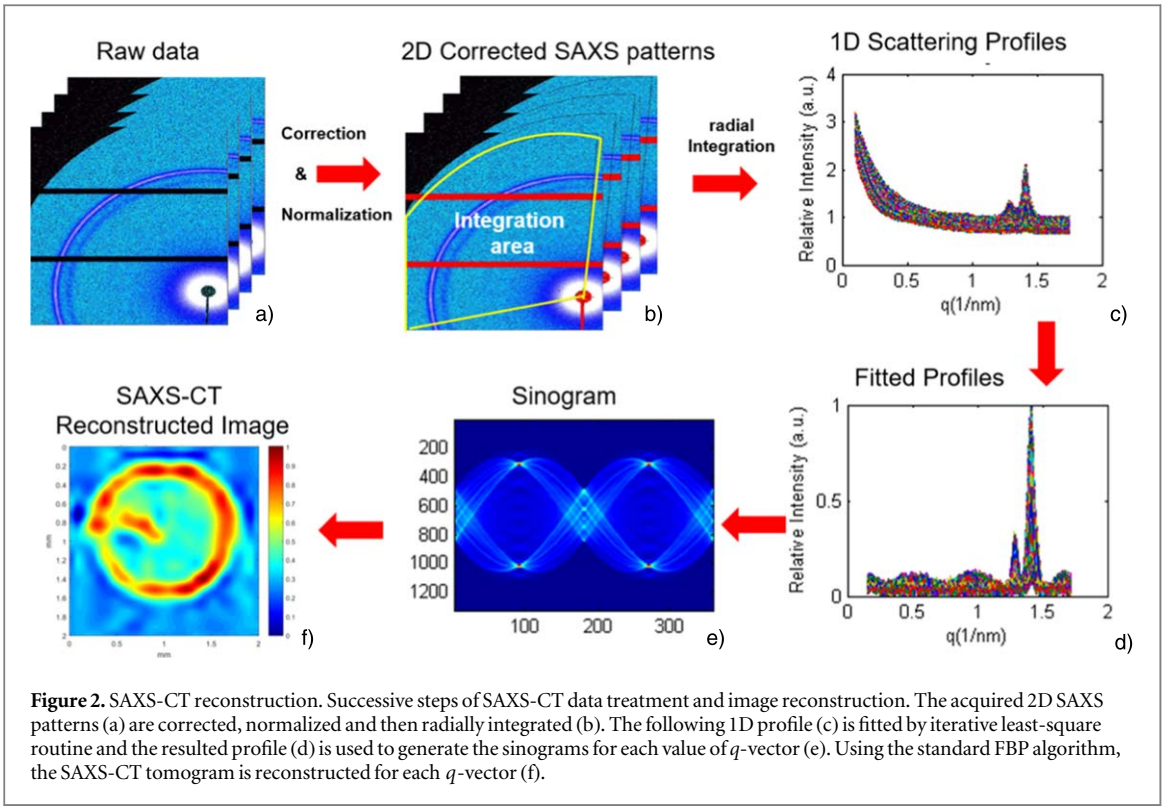

Figure 2. SAXS-CT reconstruction. Successive steps of SAXS-CT data treatment and image reconstruction. The acquired 2D SAXS patterns (a) are corrected, normalized and then radially integrated (b). The following 1D profile (c) is fitted by iterative least-square routine and the resulted profile (d) is used to generate the sinograms for each value of q-vector (e). Using the standard FBP algorithm, the SAXS-CT tomogram is reconstructed for each q-vector (f).

and detector efficiency. The corrected and normalized data were full radially integrated and transformed into a set of linear SAXS profiles. Iterative least-squares routine, based on the fitting of the exponential decay of the SAXS curves, was used to remove the intensity of the matrix where the nanostructures of interest are embedded and consequently enhance the correspondent signal of the structures of interest. Sinograms for each q-vector were calculated from the set of tailored profiles for each projection over 360°. Each projection represents scattering intensities at one q for the 16 translation steps at r-direction on figure 1(b). Finally, the local SAXS cross-section of breast specimens was reconstructed using a standard filtered back-projection (FBP) algorithm (Hamming filter) in the q_z direction, as proposed by Schroer (2006) (Schroer *et al* 2006). This approach is limited to samples that scatter nearly isotropically, where rotationally invariant is fulfilled which implies that the scattered intensity can be considered as scalar. The sample self-attenuation, calculated from the data of the pin-diodes for each projection, was used to reconstruct the attenuation coefficient $\mu(x, y)$ also using the filtered back-projection algorithm.

Reverse analysis

From the reconstructed tomogram for each q-vector, the scattering profiles at a voxel or region of interest are retrieved by the named 'reverse analysis' approach developed in this study. From the retrieved SAXS profiles, further investigations can be performed to obtain spatially localized structural information of the sample. Reverse analysis means the reconstruction of the scattering profile from a voxel or a region of interest (ROI) from the SAXS-CT tomogram. Considering the sample diameter, $d = 1.8$ mm, and the scattering angle of less than 10 mrad the path of the scattered photons is approximately equal to the path of the transmitted photons. In this case, we can retrieve the scattering profile of a defined voxel $p(x, y, q)$ applying the inverse procedure used for the image reconstruction to all q values in equation (2):

$$p(x, y, q) = \int \frac{I(x, y, q)}{I_0\, T(x, y)\, \Delta\Omega} dq \qquad (2)$$

where $T(x, y)$ is the transmission factor at (x, y) on the sample frame, resulting from the combination of the attenuation parameters before and after the local scattering, in equation (1).

Figure 3 presents an overview of the length scale range provided by the SAXS-CT nanostructure resolving microscopy. The three-dimensional SAXS tomogram reflects the distribution of x-ray scattering intensities at small angles from the macroscopic soft tissue specimen. After selection of a region of interest (ROI) in a particular slice, 1D-SAXS profiles are retrieved from each voxel within this ROI. The nanostructural information is statistically summed in each voxel and indirectly retrieved from the SAXS curves. From each spatially localized SAXS profiles, structural information about the sample under investigation can be obtained. Depending on the knowledge of the studied system, information such as lattice parameter, particle shape, size, and packing might be provided. Considering the breast specimens analyzed in this

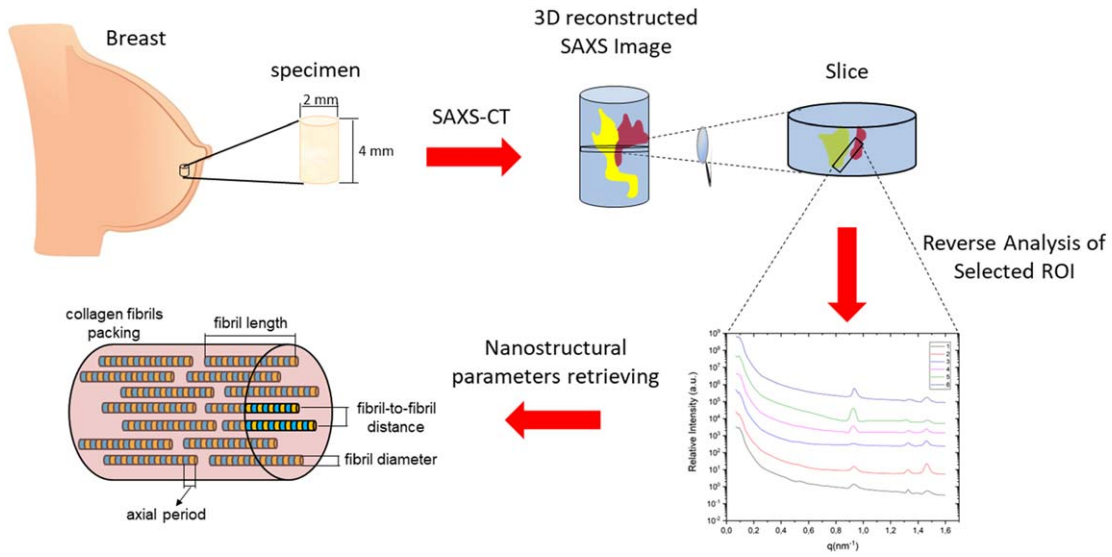

Figure 3. SAXS-CT length scale. Schematic representation of the approach for the nanostructure resolving microscopy of macroscopic soft tissue specimens. Here is presented the application on monitoring the hierarchical arrangement of fibrillar collagen in a macroscopic breast specimen. Information such as collagen fibrils packing, fibrils length, fibril diameter, fibril-to-fibril distance and axial period can be accessed.

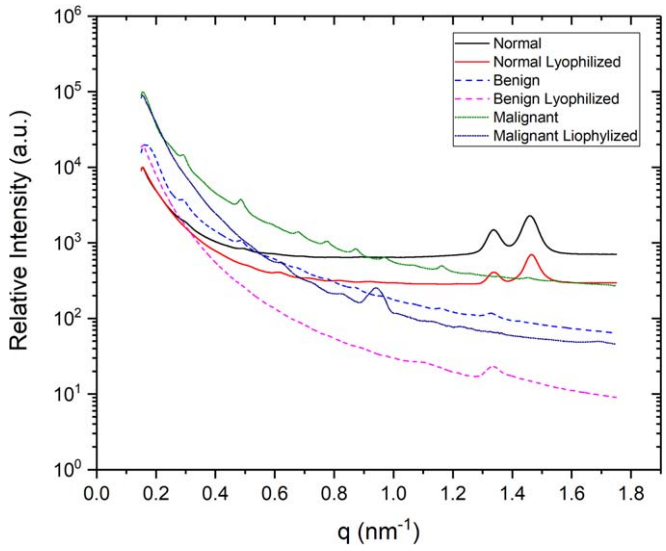

Figure 4. Comparison between the SAXS scattering profiles of normal, benign and malignant breast specimens at normal and lyophilized states.

study, collagen fibril packing, fibril diameter, fibril-to-fibril distance and axial period of fibrillar collagen could be accessed as described by Fernández *et al* (Fernández *et al* 2002). Thereby, it is possible to monitor the structural rearrangement of breast diseases concerning content and degree of alignment of collagen fibrils spatially.

However, this can be an issue because the dehydration process of the tissues can modify their inner structure, *e.g.*, collagen fibrils assemble are very sensitive to hydration. To determine the influence of water, a comparison of SAXS profiles of specimens fixed in formalin with those fixed in formalin and subsequently freeze-dried was performed.

A noticeable reduction in the intensity profiles is visualized in figure 4, indicating that the electron density contrast between the scattering structures and the matrix has been altered after dehydration. However, the similarity between the curves, i.e., the profile of each curve and the Bragg peaks, at both states (native and lyophilized) for each type of tissue reveals that the process of freeze-drying the sample conserves the tissue hierarchical and molecular integrity. The reduction in the scattered intensity is more substantial as q increase and is possibly associated with the water scattering which has a maximum intensity around momentum transfer of 20 nm^{-1} (Conceição *et al* 2019).

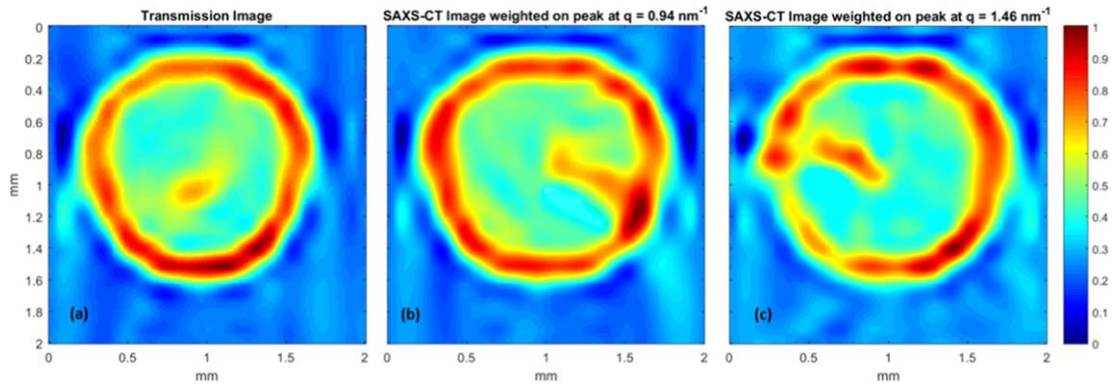

Figure 5. Comparison between transmission and small-angle scattering images. (a) reconstructed transmission image; (b) SAXS-CT reconstructed image for the specific momentum transfer ($q_1 = 0.94\ nm^{-1}$) and, (c) for the momentum transfer ($q_2 = 1.46\ nm^{-1}$). The color bar label '1' refers to the highest scattered photons intensity, while '0' indicates no detectable scattered photons at the respective position in linear scale.

Our previous studies (Conceição *et al* 2009) have shown three general features in the SAXS profiles common to normal and pathological human breast specimens which can also be identified here from dried samples: (i) exponential decay is dependent of the type of breast tissue, which might be associated with changes in the tissue microenvironment, specifically in the extracellular matrix (Clark and Vignjevic 2015) (ii) several peaks between 0.25 nm^{-1} and 1.17 nm^{-1} reflecting higher order of collagen fibril reflections related to type I collagen (Fernández *et al* 2002) and (iii) two broad peaks, at q = 1.33 nm^{-1} and q = 1.46 nm^{-1}, highlighting the adipose content of the sample (Sidhu *et al* 2011), which is supposed to be correspondent to a lipoprotein with a long hydrocarbon chain (Tartari *et al* 1997) and the packing of triglycerides (Conceiçao *et al* 2010), respectively. As expected, the collagen peaks intensity are more pronounced in the scattering profile of malignant tumor (Ductal Invasive Carcinoma) than normal tissue or benign tumor (Fibroadenoma) (Fernández *et al* 2002). In this case, it occurs a realignment of the collagen fibrils that allow individual tumor cells to migrate out along radially aligned fibers (Provenzano *et al* 2006, 2008, Nie *et al* 2015). In addition, the transition from the hydrated to a dry state, there are four main events affecting collagen fibrils: (a) the decrease of the fundamental periodicity of the collagen fibrils (Wess and Orgel 2000) from 63.9 ± 0.3 nm for all types of tissue to 61.8 ± 0.3 nm, 62.8 ± 0.4 nm and 59.7 ± 0.3 for normal, benign and malignant specimens, respectively; (b) the broadening of the collagen peaks, which is related to portions of collagen chains adopting a tilt to the fiber axis (Wess and Orgel 2000), (c) the 9th order (q = 0.94 nm^{-1}) of the axial period dominates all others, which implies a periodicity of 6.7 nm, and (d) despite the shift in the meridional collagen diffraction (Andriotis *et al* 2015), the peak at lowest *q* related to the packing of these fibrils (Suhonen *et al* 2005) are not detectably altered by the changes in the hydration as also observed for collagen fibrils in cornea stroma (Fratzl and Daxer 1993).

Results

Mapping the local nanostructures

Despite some inter- and intra-collagen fibril changes, the architectural tissue packing is not affected by sample preparation as evidenced by the lowest-q peak intensity. Indeed, after drying, the main features of adipose and fibroglandular tissues are enhanced, *e.g.*, collagen (9th order reflection) and triglycerides (d-spacing = 43 Å). Thereby, this benefit was used to monitor the distribution of these structures within the assembly and based on the relation between adipose and fibroglandular content (Griffiths *et al* 2007, Conceição *et al* 2011); the normal, benign and malignant portions were localized.

The reconstructed transmission image is shown in figure 5(a). Since the attenuation coefficients of normal, benign and malignant human breast tissues are very similar at the x-ray energy used in this experiment (Tomal *et al* 2010), the tomographic image generated by transmission has not enough contrast to differentiate the specimens. A slight localized rise of intensity is observed in the intersection region between the samples, which is filled by air. Moreover, no information on the micro- and nano-structure of the tissues can be accessed. Based on the remarkable characteristics of each type of breast tissue in the scattering profiles showed in figure 3, the distribution of the collagen fibrils (q = 0.94 nm^{-1}) and the triglycerides (q = 1.46 nm^{-1}) in a single tomography slice through the sample assembly was reconstructed and is presented in figures 4(b) and (c), respectively. In figure 5(b) a high density of aligned collagen is observed exactly in the region corresponding to the ductal invasive carcinoma. In this type of malignant tumor, generally, the stroma undergoes a desmoplastic reaction characterized by over-deposition of

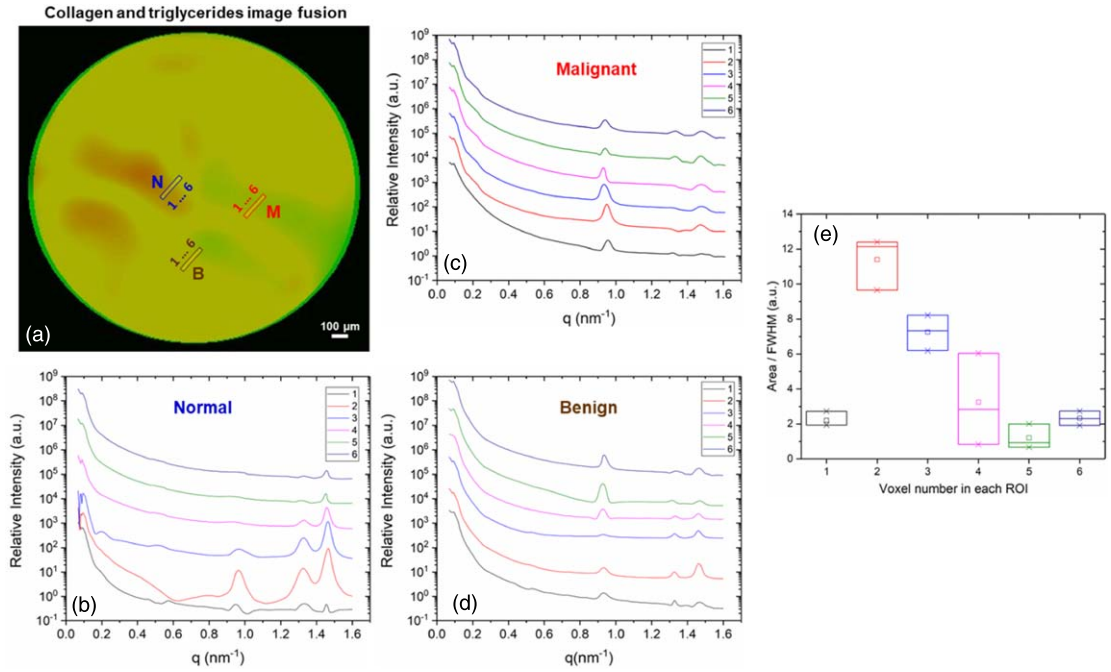

Figure 6. Spatially monitoring of nanostructures by reverse analysis. (a) Image fusion of the SAXS tomograms for the momentum transfers q = 0.94 nm^{-1} and q = 1.46 nm^{-1}; orange regions correspond to triglycerides while the green ones to collagen fibril deposition. (b), (c) and (d) present the recovered SAXS scattering profiles from the region of interest defined by the rectangles in figure 6(a). The labels from 1 to 6 are used to indicate the position of voxels in the selected ROI as well as N, B and M refer to normal, benign and malignant, respectively. For clarity, each curve has an offset of 10x to each other. (e) Distribution of the ratio between area and FWHM of the collagen peak for the ROI labeled as M and two parallel ROIs neighboring it left and right. As higher the ratio between the peak area and the FWHM as more collagen content and organized are the fibrils' packing.

bundles of type I and III collagens localized at the invasion front of the tumor. This behavior is highlighted by the collagen fibril concentration at the lower-left portion of the malignant specimen, indicating the tumor spread pathway. There is no visible collagen buildup over the health and benign lesion specimens. For fibroadenoma, although collagen content surrounding the ducts increases, the fibers are randomly distributed (Nie *et al* 2015), which implies a near washout of the corresponding SAXS intensity. Figure 5(c) presents the distribution of triglycerides on the sample assembly. Noticeably, the triglycerides, which are synthesized by white adipose tissue(Ahmadian *et al* n.d.), are clustered at the upper left part of the sample assembly, precisely where the normal tissue is. Although malignant and nonmalignant human breast neoplasms grow in the anatomical vicinity of adipose tissue in this study the pathological specimens were cut to be as homogeneous as possible to enable being structurally characterized. Thereby the presence of triglycerides is virtually nonexistent in these specimens.

Nanostructural survey

Based on the previous study (Conceição *et al* 2009), the nanostructures present in health and pathological human breast tissues are labeled, as due to type I collagen fibril (peak at q = 0.94 nm^{-1}) and as associated to the packing of triglycerides (peak at q = 1.46 nm^{-1}). However, in the case of a specimen with no prior information, the identification might be achieved *a posteriori* from information such as lattice parameter, molecular shape and packing in defined parts of the sample. These features can be obtained using the reverse analysis procedure (Bleuet *et al* 2008, Jensen *et al* 2011). Although the distribution of collagen fibrils and triglycerides can be visualized in figures 5(b) and (c), the architectural rearrangement of their units cannot be accessed unless applying reverse analysis. Figures 6(b), (c) and (d) exhibit the retrieved scattering profiles for the selected regions-of-interest (ROIs) shown in figure 6(a) corresponding to regions on normal, malignant and benign tissues, respectively. The image generated by merging the SAXS tomograms at $q_z = 0.94\ nm^{-1}$ at $q_z = 1.46\ nm^{-1}$ is presented in figure 6(a). Reverse analysis was applied on the six voxels included in each ROI on the figure 6(a). From the figure 6(b) it is observed the scattering from the packing of triglycerides standing out in the SAXS 1D profiles from the normal portion of the sample assembly. Likewise type I collagen dominates the scattering profiles of the benign and malignant lesions, figures 6(b) and (c), respectively. By fitting Gaussian peaks at $q = 1.46\ nm^{-1}$ and at $q = 0.94\ nm^{-1}$, parameters like peak area and FWHM are extracted. From the ratio between these parameters, changes in the molecular nanostructure as well as in the degree of organization of their packing (Fernández *et al* 2002, Suhonen *et al* 2005) are identified.

Concerning the Ductal Invasive Carcinoma behavior, the occurrence of an over-deposition of bundles

of type I localized at the invasion front of a tumor has been reported (Provenzano *et al* 2006, Morris *et al* 2016). To evaluate this behavior, two ROIs comprising six voxels each were analyzed neighboring left and right parallel to the red rectangle in figure 6(a). The peaks at $q = 0.94\ \mathrm{nm}^{-1}$ in all retrieved SAXS profiles were fitted as Gaussian peaks. Peak area and FWHM were determined and shown in figure 6(e), illustrating the variation of collagen content and organization crossing the invasion front region. Voxels two and three are fully immersed within the tumor invasion region, which is visibly by stronger scattering arising from areas invaded by cancer, corresponding to a large increase of the specific surface area of the collagen fibrils (Fernández *et al* 2002).

Despite the possibility to perform a more comprehensive exploration of the changes in the nanostructure parameters of collagen fibrils (Fernández *et al* 2002), it requires integration on parallel and perpendicular directions to the preferential collagen fiber axis from the SAXS pattern, which was out of the scope of this study. Herein, the focus is on the ability of SAXS-CT to directly identify alterations and monitor a specific nanostructure spatially with a large field-of-view.

Discussion

SAXS can probe nanostructural biomolecules with sizes ranging from a few kilo-Daltons to several mega-Daltons (Feigin and Svergun 1987), the applicability to investigate large conformational transitions is immense, related to content and degree of self-organization of these macromolecules through a macroscopic specimen. In particular, for breast tumors, growth, progression and metastasis are controlled by the tumor microenvironment. Thereby, a three-dimensional inspection of specific biomolecules in the extracellular matrix (ECM) such as collagen fibril (Kauppila *et al* 1998, Brown *et al* 2003), fibroblasts (Kalluri and Zeisberg 2006) and adipocytes (Nieman *et al* 2013) undoubtedly contributes to elucidate those process. The pattern of collagen intercellular arrangement enables one to foresee the prognostic of the disease based on the tumor-associated collagen signatures (TACS) (Provenzano *et al* 2006, 2008). Cancer-associated fibroblasts (CAFs) have been considered as synthetic machines responsible for creating extracellular matrix (ECM) structure and metabolic and immune reprogramming of the tumor microenvironment with an impact on adaptive resistance to chemotherapy (Kalluri and Zeisberg 2006). Adipocytes dedifferentiate into pre-adipocytes or are reprogrammed into cancer-associated adipocytes (CAA) during their interaction with cancer cells (Nieman *et al* 2013). SAXS-CT enables access and maps these individual key molecules which supply basis to improve the knowledge on the multiple interactions between them and their functional role. Nevertheless, it is worth mentioning this survey relies on assigned peaks by some *a priori* knowledge about the sample.

In summary, the SAXS-CT approach presented here overcomes both the limitations of the current microscopy techniques and offers the possibility to access and monitor the nanostructures in macroscopic soft tissue specimens without the requirement of any dye. Their application on investigating normal and pathological human breast specimens shed light on the hallmarks of the adipose and fibroglandular breast tissues, triglycerides and collagen fibril respectively. Based on the spatial distribution of these hallmarks, normal, benign and malignant human breast specimens were identified within the sample assembly, as previously used to characterize normal and neoplastic human breast specimens (Conceição *et al* 2009, 2011). Additionally, monitoring the structural rearrangements of collagen fibrils through the sample, based on the retrieved scattering profiles from different regions of interest, insights about the direction of cancer spread are obtained by the higher content and degree of organization. Finally, it is expected that this approach using SAXS-CT in soft tissue provides a path to high-resolution nanostructural probe with a large field-of-view and its impact on structural biology, tissue engineering and medicine will be tremendous.

Acknowledgments

The authors would like to recognize and thank the technical assistance of the SAXS2 beamline staff during the experiments in the National Synchrotron Light Laboratory (LNLS) in Campinas, Brazil. A L C C special thanks to the contribution of Prof. Martin Poletti from FFCLRP-USP during the SAXS experiment at LNLS. A L C C also appreciated the guidance of Dr Andre Rothkirch from DESY during the development of the reconstruction algorithm. Also, we also would like to thank the Department of Pathology of the Clinics Hospital, Faculty of Medicine of Ribeirão Preto, Brazil, for the collection and conduction of the histopathological analysis of the human breast specimens investigated in this study. In particular, Prof. Alfredo Ribeiro-Silva. This research had the financial support of the São Paulo Research Foundation (FAPESP) under project number (2011/20632-6).

Competing interest

The authors declare that they have no competing interests.

ORCID iDs

A L C Conceição https://orcid.org/0000-0002-1693-5295
J Perlich https://orcid.org/0000-0002-3378-2710
S Haas https://orcid.org/0000-0001-7066-0205

References

Andriotis O G, Chang S W, Vanleene M, Howarth P H, Davies D E, Shefelbine S J, Buehler M J and Thurner P J 2015 Structure-mechanics relationships of collagen fibrils in the osteogenesis imperfecta mouse model *J. R. Soc. Interface* **12** 20150701

Antoniassi M, Conceição A L C and Poletti M E 2014 Rayleigh to compton ratio scatter tomography applied to breast cancer diagnosis: a preliminary computational study *Radiat. Phys. Chem.* **95** 288–91

Bleuet P, Welcomme E, Dooryhée E, Susini J, Hodeau J-L and Walter P 2008 Probing the structure of heterogeneous diluted materials by diffraction tomography *Nat. Mater.* **7** 468–72

Brown E, McKee T, diTomaso E, Pluen A, Seed B, Boucher Y and Jain R K 2003 Dynamic imaging of collagen and its modulation in tumors *in vivo* using second-harmonic generation *Nat. Med.* **9** 796–800

Chantrill L A *et al* 2015 Precision medicine for advanced pancreas cancer: the individualized molecular pancreatic cancer therapy (IMPaCT) Trial *Clin Cancer Res* **21** 2029–37

Clark A G and Vignjevic D M 2015 Modes of cancer cell invasion and the role of the microenvironment *Curr. Opin. Cell Biol.* **36** 13–22

Conceição A L C, Antoniassi M, Cunha D M, Ribeiro-Silva A and Poletti M E 2011 Multivariate analysis of the scattering profiles of healthy and pathological human breast tissues *Nucl. Instruments Methods Phys. Res. Sect. A Accel. Spectrometers, Detect. Assoc. Equip.* **652** 870–3

Conceiçao A L C, Antoniassi M and Poletti M E 2010 Assessment of the differential linear coherent scattering coefficient of biological samples *Nucl. Instruments Methods Phys. Res. Sect. A Accel. Spectrometers, Detect. Assoc. Equip.* **619** 67–70

Conceição A L C, Antoniassi M and Poletti M E 2009 Analysis of breast cancer by small angle x-ray scattering (SAXS) *Analyst* **134** 1077

Conceição A L C, Meehan K, Antoniassi M, Piacenti-Silva M and Poletti M E 2019 The influence of hydration on the architectural rearrangement of normal and neoplastic human breast tissues *Heliyon* **5** e01219

Feigin L A and Svergun D I 1987 *Structure Analysis by Small-Angle X-Ray and Neutron Scattering* ed G W Taylor (Boston, MA, US: Springer) (http://link.springer.com/10.1007/978-1-4757-6624-0)

Feldkamp J M, Kuhlmann M, Roth S V, Timmann A, Gehrke R, Shakhverdova I, Paufler P, Filatov S K, Bubnova R S and Schroer C G 2009 Recent developments in tomographic small-angle x-ray scattering *Phys. Status Solidi* **206** 1723–6

Fernández M, Keyriläinen J, Serimaa R, Torkkeli M, Karjalainen-Lindsberg M-L, Tenhunen M, Thomlinson W, Urban V and Suortti P 2002 Small-angle x-ray scattering studies of human breast tissue samples *Phys. Med. Biol.* **47** 577–92

Fratzl P 2015 Imaging techniques: extra dimension for bone analysis *Nature* **527** 308–9

Fratzl P and Daxer A 1993 Structural transformation of collagen fibrils in corneal stroma during drying. An x-ray scattering study *Biophys. J.* **64** 1210–4

Georgiadis M, Guizar-Sicairos M, Zwahlen A, Trüssel A J, Bunk O, Müller R and Schneider P 2015 3D scanning SAXS: a novel method for the assessment of bone ultrastructure orientation *Bone* **71** 42–52

Graham S J, Stanchev P L, Lloyd-Smith J O A, Bronskill M J and Plewes D B 1995 Changes in fibroglandular volume and water content of breast tissue during the menstrual cycle observed by MR imaging at 1.5 t *J. Magn. Reson. Imaging* **5** 695–701

Griffiths J A, Royle G J, Hanby A M, Horrocks J A, Bohndiek S E and Speller R D 2007 Correlation of energy dispersive diffraction signatures and microCT of small breast tissue samples with pathological analysis *Phys. Med. Biol.* **52** 6151–64

Huang P, Wang D, Su Y, Huang W, Zhou Y, Cui D, Zhu X and Yan D 2014 Combination of small molecule prodrug and nanodrug delivery: amphiphilic drug–drug conjugate for cancer therapy *J. Am. Chem. Soc.* **136** 11748–56

Isenberg B C and Wong J Y 2006 Building structure into engineered tissues *Mater. Today* **9** 54–60

Jackson S E and Chester J D 2015 Personalised cancer medicine *Int. J. Cancer* **137** 262–6

Jennings T A 1999 *Lyophilization: introduction and basic principles* (Interpharm Press)

Jensen T H, Bech M, Bunk O, Thomsen M, Menzel A, Bouchet A, Le Duc G, Feidenhans'l R and Pfeiffer F 2011 Brain tumor imaging using small-angle x-ray scattering tomography *Phys. Med. Biol.* **56** 1717–26

Jorba I, Uriarte J J, Campillo N, Farré R and Navajas D 2017 Probing micromechanical properties of the extracellular matrix of soft tissues by atomic force microscopy *J. Cell. Physiol.* **232** 19–26

Kalluri R and Zeisberg M 2006 Fibroblasts in cancer *Nat. Rev. Cancer* **6** 392–401

Kauppila S, Stenbäck F, Risteli J, Jukkola A and Risteli L 1998 Aberrant type I and type III collagen gene expression in human breast cancer *in vivo J. Pathol.* **186** 262–8

Liebi M *et al* 2018 Small-angle x-ray scattering tensor tomography: model of the three-dimensional reciprocal-space map, reconstruction algorithm and angular sampling requirements *Acta Crystallogr. Sect. A Found. Adv.* **74** 12–24

Liebi M, Georgiadis M, Menzel A, Schneider P, Kohlbrecher J, Bunk O and Guizar-Sicairos M 2015 Nanostructure surveys of macroscopic specimens by small-angle scattering tensor tomography *Nature* **527** 349–52

Manohar N, Reynoso F J, Diagaradjane P, Krishnan S and Cho S H 2016 Quantitative imaging of gold nanoparticle distribution in a tumor-bearing mouse using benchtop x-ray fluorescence computed tomography *Sci. Rep.* **6** 22079

Morris B A, Burkel B, Ponik S M, Fan J, Condeelis J S, Aguirre-Ghiso J A, Castracane J, Denu J M and Keely P J 2016 Collagen matrix density drives the metabolic shift in breast cancer cells *EBio Medicine* **13** 146–56

National Research Council (US) Committee on a Framework for Developing a New Taxonomy of Disease 2011 *Toward Precision Medicine: Building a Knowledge Network for Biomedical Research and a New Taxonomy of Disease* (National Academies Press)

Nie Y T, Wu Y, Fu F M, Lian Y E, Zhuo S M, Wang C and Chen J X 2015 Differentiating the two main histologic categories of fibroadenoma tissue from normal breast tissue by using multiphoton microscopy *J. Microsc.* **258** 79–85

Nieman K M, Romero I L, Van Houten B and Lengyel E 2013 Adipose tissue and adipocytes support tumorigenesis and metastasis *Biochim. Biophys. Acta - Mol. Cell Biol. Lipids* **1831** 1533–41

Peddie C J and Collinson L M 2014 Exploring the third dimension: volume electron microscopy comes of age *Micron* **61** 9–19

Png G M, Choi J W, Ng B W-H, Mickan S P, Abbott D and Zhang X-C 2008 The impact of hydration changes in fresh bio-tissue on THz spectroscopic measurements *Phys. Med. Biol.* **53** 3501–17

Provenzano P P, Eliceiri K W, Campbell J M, Inman D R, White J G and Keely P J 2006 Collagen reorganization at the tumor-stromal interface facilitates local invasion *BMC Med.* **4** 38

Provenzano P P, Inman D R, Eliceiri K W, Knittel J G, Yan L, Rueden C T, White J G and Keely P J 2008 Collagen density promotes mammary tumor initiation and progression *BMC Med.* **6** 1–15

Romanov V, Grubsky V and Zahiri F 2017 Compton imaging tomography for nondestructive evaluation of large multilayer aircraft components and structures *AIP Conf. Proc.* vol 1806AIP Publishing LLC) p130001

Roth S V, Döhrmann R, Dommach M, Kuhlmann M, Kröger I, Gehrke R, Walter H, Schroer C, Lengeler B and Müller-Buschbaum P 2006 Small-angle options of the upgraded ultrasmall-angle x-ray scattering beamline BW4 at HASYLAB *Rev. Sci. Instrum.* **77** 085106

Schaff F, Bech M, Zaslansky P, Jud C, Liebi M, Guizar-Sicairos M and Pfeiffer F 2015 Six-dimensional real

and reciprocal space small-angle x-ray scattering tomography *Nature* **527** 353–6
Schroer C G, Kuhlmann M, Roth S V, Gehrke R, Stribeck N, Almendarez-Camarillo A and Lengeler B 2006 Mapping the local nanostructure inside a specimen by tomographic small-angle x-ray scattering *Appl. Phys. Lett.* **88** 164102
Sharma Y, Wieczorek M, Schaff F, Seyyedi S, Prade F, Pfeiffer F and Lasser T 2016 Six dimensional x-ray tensor tomography with a compact laboratory setup *Appl. Phys. Lett.* **109** 134102
Sidhu S, Falzon G, Hart S A, Fox J G, Lewis R A and Siu K K W 2011 Classification of breast tissue using a laboratory system for small-angle x-ray scattering (SAXS) *Phys. Med. Biol.* **56** 6779–91
Skjønsfjell E T, Kringeland T, Granlund H, Høydalsvik K, Diaz A, Breiby D W and IUCr 2016 Retrieving the spatially resolved preferred orientation of embedded anisotropic particles by small-angle x-ray scattering tomography *J. Appl. Crystallogr.* **49** 902–8
Stribeck N, Camarillo A A, Nöchel U, Schroer C, Kuhlmann M, Roth S V, Gehrke R and Bayer R K 2006 Volume-resolved nanostructure survey of a polymer part by means of SAXS microtomography *Macromol. Chem. Phys.* **207** 1139–49
Stribeck N, Nöchel U, Fakirov S, Feldkamp J, Schroer C, Timmann A and Kuhlmann M 2008 SAXS-fiber computer tomography. Method enhancement and analysis of microfibrillar-reinforced composite precursors from PEBA and PET *Macromolecules* **41** 7637–47
Suhonen H, Fernández M, Serimaa R and Suortti P 2005 Simulation of small-angle x-ray scattering from collagen fibrils and comparison with experimental patterns *Phys. Med. Biol.* **50** 5401–16
Tartari A, Casnati E, Bonifazzi C and Baraldi C 1997 Molecular differential cross sections for x-ray coherent scattering in fat and polymethyl methacrylate *Phys. Med. Biol.* **42** 2551–60
Tomal A, Mazarro I, Kakuno E M and Poletti M E 2010 Experimental determination of linear attenuation coefficient of normal, benign and malignant breast tissues *Radiat. Meas.* **45** 1055–9
Wess T J and Orgel J P 2000 Changes in collagen structure: drying, dehydrothermal treatment and relation to long term deterioration *Thermochim. Acta* **365** 119–28
Zierold K 1988 X-ray microanalysis of freeze-dried and frozen-hydrated cryosections *J. Electron Microsc. Tech.* **9** 65–82